ANL/MSD/CP--83776
Conf-950228--6

Epitaxial $Pb(Zr_xTi_{1-x})O_3/SrRuO_3$ (x = 0, 0.35, 0.65) Multilayer Thin Films on $SrTiO_3$(100) and MgO(100) Prepared by MOCVD and RF Sputtering*

C. M. Foster, R. Csencsits, P. M. Baldo, G. R. Bai, Z. Li, and L. E. Rehn
Materials Science Division, Argonne National Laboratory
9700 S. Cass Avenue, Argonne, IL. 60439

L. A. Wills and R. Hiskes
Hewlett-Packard Laboratory, Hewlett-Packard Company
3500 Deer Creek Road, Palo Alto, CA. 94304

February 1995

Manuscript to be presented at the 1995 North American Conference on Smart Structures and Materials, San Diego, CA, February 26-March 3, 1995; to be published in the SPIE Proceedings.

*The work at ANL was supported by the U.S. Department of Energy, Basic Energy Sciences-Materials Sciences, under contract #W-31-109-ENG-38 under the joint CRADA with Hewlett-Packard Company #C9301701.

Epitaxial $Pb(Zr_xTi_{1-x})O_3/SrRuO_3$ (x=0, 0.35, 0.65) multilayer thin films on $SrTiO_3(100)$ and MgO(100) prepared by MOCVD and RF sputtering

C. M. Foster, R. Csencsits, P. M. Baldo, G. R. Bai, Z. Li, and L. E. Rehn

Materials Science Division, Argonne National Laboratory
9700 S. Cass Avenue, Argonne, IL 60439

L. A. Wills and R. Hiskes

Hewlett Packard Laboratories, Hewlett-Packard Company
3500 Deer Creek Road, Palo Alto, CA 94304

ABSTRACT

Epitaxial $SrRuO_3$ thin films were deposited on $SrTiO_3(100)$ and MgO(100) substrates by RF sputtering for use as bottom electrodes and epitaxial buffer layers. On these conductive substrates, epitaxial $Pb(Zr_xTi_{1-x})O_3$ (PZT; x=0.35,0.65) and $PbTiO_3$ (PT; x=0) thin films were deposited by metalorganic chemical vapor deposition (MOCVD). X-ray diffraction (XRD), RBS channeling (RBS), transmission electron microscopy (TEM) and optical waveguiding were used to characterize the phase, microstructure, defect structure, refractive index, and film thickness of the deposited films. The PZT and PT films were epitaxial and c-axis oriented. 90° domains, interfacial misfit dislocations and threading dislocations were the primary structural defects, and the films showed as high as a 70% RBS channeling reduction. Ferroelectric hysteresis and dielectric measurements of epitaxial PZT ferroelectric capacitor structures formed using evaporated Ag top electrode showed: a remanent polarization of 46.2 $\mu C/cm^2$, a coercive field of 54.9 kV/cm, a dielectric constant of 410, a bipolar resistivity of ~5.8×10^9 Ω-cm at a field of 275 kV/cm, and a breakdown strength of >400 kV/cm. Cyclic fatigue measurements showed that the remanent polarization was maintained for >10^9 cycles.

1. INTRODUCTION

Current interest in ferroelectric thin films results from the numerous potential applications for these materials which utilize the unique dielectric, pyroelectric, electro-optic, acousto-optic, and piezo-electric properties of ferroelectrics materials[1]. The synthesis of thin films of the lead-based ferroelectrics, $PbTiO_3$, $Pb(Zr_xTi_{1-x})O_3$ (PZT), $(Pb_{1-x}La_x)(Zr_yTi_{1-y})O_3$ (PLZT), etc., using a variety of techniques (e. g., sol-gel, sputtering, laser ablation, MOCVD) and the resulting properties of the films have been studied extensively[1]. For many applications, such as non-volatile dynamic random access memory (DRAM) or electro-optic waveguide modulators, a highly textured microstructure is preferable or essential. Ferroelectric film deposition using MOCVD has been widely reported and has been shown to be able to produce film microstructures from random polycrystalline to highly epitaxial[2]. Devices fabricated from single-crystal films with low defect density could potentially take full advantage of the tensor nature of the anisotropic properties

of ferroelectric materials, resulting in improved device performance and enhanced device characteristics. In addition, for applications such as optical waveguide modulators, waveguide frequency doublers and Surface Acoustic Wave (SAW) delay lines, the high degree of structural perfection in such epitaxial films could substantially reduce propagation losses associated with grain boundary scattering to levels where the total insertion losses are sufficiently low (i. e., <1.0 dB/cm) for feasible device applications.

We have systematically studied the effects of gas phase composition, substrate materials, substrate orientation, and deposition temperature on the phase, composition, crystallinity, morphology and domain structure of epitaxial thin films of $PbTiO_3$[3-5]. We have also discussed the effects of the choice of substrate material on the crystallinity, microstructure, domain formation, defect structure and optical properties of $PbTiO_3$ thin films[6-7]. In this paper, we report results on the growth, characterization and properties of $Pb(Zr_{0.35}Ti_{0.65})O_3$, $Pb(Zr_{0.65}Ti_{0.35})O_3$ and $PbTiO_3$ thin films deposited on $SrRuO_3$ buffered $SrTiO_3$(100) and MgO(100) substrates using MOCVD. These results demonstrate that near single-crystal-like structure and dielectric properties can be achieved in epitaxial PZT thin film multilayer structures.

2. EXPERIMENTAL

Epitaxial $SrRuO_3$ thin films were deposited on epitaxial-grade (100) $SrTiO_3$ and MgO (100) substrates by 90° off-axis, RF magnetron sputtering at a growth pressure of 15 Pa and deposition temperature of 650°C. Sputter deposition commenced at a power of 60W and a Ar/O_2 flow rate of 120/80 sccm. The growth rate of the $SrRuO_3$ layers was estimated from RBS to be ~160Å per hour. For MgO (100) substrates, the same growth conditions were used, however, an additional $BaTiO_3$ (100) buffer layer was used between the $SrRuO_3$ and the MgO substrate to improve the crystallinity of the $SrRuO_3$ [8].

PZT and PT thin film depositions were carried out in a low pressure, horizontal, cold wall reactor with a resistive substrate heater. The $SrRuO_3$ buffered $SrTiO_3$(100) and MgO (100) were used as the substrate materials. Tetraethyl lead, $Pb(C_2H_5)_4$, zirconium t-butoxide, $Zr(OC(CH_3)_3)_4$, and titanium isopropoxide, $Ti(OC_3H_7)_4$, (Morton International, Advanced Materials, Danvers, MA) were chosen as the metal ion precursors. UHP (99.9995%) N_2 and O_2 were used as the carrier gas and the oxidant, respectively. Details of the reactor design and deposition methods have been previously reported[3-7,9]. The growth conditions for deposition of $PbTiO_3$, $Pb(Zr_{0.35}Ti_{0.65})O_3$ and $Pb(Zr_{0.65}Ti_{0.35})O_3$ are shown in Table I.

The crystallinity, domain structure and chemical composition of the $PbTiO_3$ films were investigated with x-ray diffraction (XRD) analysis. X-ray θ-2θ diffraction and θ-rocking spectra of the films were obtained using a Rigaku diffractometer and a 15 kW $Cu_{K\alpha}$ rotating anode x-ray source. The angular resolution of this system is 2θ & θ >0.10°, χ ~3.5°. Crystallographic analysis and off-specular XRD was performed using a 12 kW $Cu_{K\alpha}$ rotating anode x-ray source focused by a bent graphite monochromator to the center of a four-circle Huber spectrometer. A two-circle stage with a second graphite analyzer was mounted on the 2θ arm. The angular resolution of this system is 2θ & θ ~0.15°, φ ~0.17-0.50°, χ ~0.9-1.5°. A detailed description of this 6-circle XRD system and its application to the study of epitaxial thin films is given elsewhere[10]. Descriptions of the TEM sample preparation and methods have been previously reported[3-4]. The RBS and channeling methods as well as details of the ion-channeling apparatus have been described previously[11]. Prism-coupling waveguide experiments were performed with a Metricon 2010 Prism-Film

TABLE I. GROWTH CONDITIONS

Substrate temperature	700°C
Reactor pressure	8 torr
OM precursor temperature	$Ti(OC_3H_7)_4$ - 39-40 °C $Pb(C_2H_5)_4$ - 27-28 °C $Zr(OCH_3)_4$ - 29-30 °C
OM precursor pressure	$Ti(OC_3H_7)_4$ - 37 torr $Pb(C_2H_5)_4$ - 150 torr $Zr(OC(CH_3)_3)_4$ - 400 torr
Flow rate of reactant gas (O_2)	200 sccm
Flow rate of OM and carrier gas (N_2) $PbTiO_3$	$Ti(OC_3H_7)_4$ - 50 sccm $Pb(C_2H_5)_4$ - 35 sccm $Zr(OC(CH_3)_3)_4$ - 0 sccm
Flow rate of OM and carrier gas (N_2) $Pb(Zr_{0.35}Ti_{0.65})O_3$	$Ti(OC_3H_7)_4$ - 35 sccm $Pb(C_2H_5)_4$ - 50 sccm $Zr(OC(CH_3)_3)_4$ - 25 sccm
Flow rate of OM and carrier gas (N_2) $Pb(Zr_{0.65}Ti_{0.35})O_3$	$Ti(OC_3H_7)_4$ - 35 sccm $Pb(C_2H_5)_4$ - 50 sccm $Zr(OC(CH_3)_3)_4$ - 25 sccm
Flow rate of background gas (N_2)	600 sccm
Film thickness	0.2-1.0 μm
Film growth rate	40 Å/min.
Substrates	$SrRuO_3/SrTiO_3$ (100), $SrRuO_3/BaTiO_3/MgO$(100)

coupler using a HeNe laser (632.8 nm); this system has been described elsewhere[9]. Ferroelectric hysteresis, bipolar resistance, dielectric fatigue, and dielectric breakdown measurement were obtained using a Radiant Technologies RT6000HVS tester.

3. RESULTS AND DISCUSSION

Epitaxial metallic oxide layers have been show to yield enhanced device performance due to their excellent chemical and structural compatibility with many oxide materials[12]. The growth of $SrRuO_3$ and other conductive oxide thin films for use as buffer layers and epitaxial electrodes has shown great promise in the field of integrated ferroelectrics because of the significant improvement in fatigue characteristic of capacitors formed using these electrodes[13]. In Fig. 1, we show the results of four-circle XRD on an epitaxial $SrRuO_3$ thin film deposited on $SrTiO_3$(100) by RF sputtering. The thickness of the layer was ~330Å determined by RBS and TEM measurements. In Fig. 1a, we show the specular θ-2θ scan. In addition to the $SrTiO_3$ (100) and (200) substrate reflections, the only observable reflections correspond to $SrRuO_3$ (100) and (200). The θ-rocking curves for $SrTiO_3$ (100) and $SrRuO_3$ (200) are show in Fig. 1b; the full width at half maximum (FWHM) of the $SrRuO_3$ (200) reflection, which determines that the crystalline mosaic spread of

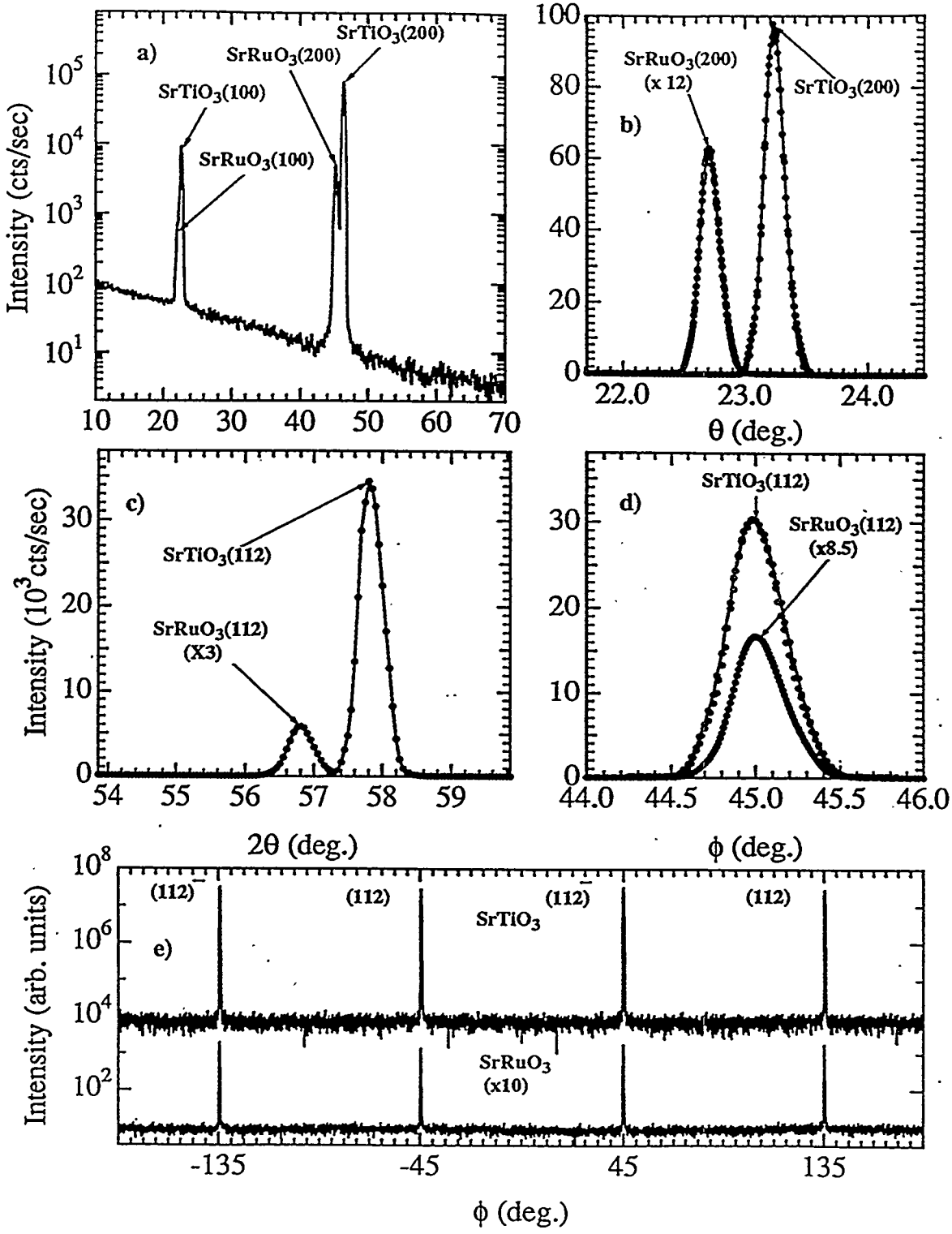

Figure 1: XRD data for a $SrRuO_3$ thin film deposited on $SrTiO_3$ (100) by RF sputtering: a) specular θ-2θ scan, b) θ-rocking of $SrRuO_3$ (200) and $SrTiO_3$ (200), c) offspecular θ-2θ scan of $SrRuO_3$ (112) and $SrTiO_3$ (112), d) detailed ϕ-scan of $SrRuO_3$ (112) and $SrTiO_3$ (112), e) 360° ϕ-scans.

the growth plane, is ~0.15° (instrument resolved) and is comparable to that of the substrate reflection. Fig. 1c and 1d, show the off-specular θ-2θ scan and φ-scans, respectively, of the $SrTiO_3$ (112) and $SrRuO_3$ (112) reflections. In Fig. 1c, the presence of the $SrRuO_3$ (112) reflection oriented with respect to the $SrTiO_3$ (112) reflection indicates the single crystal nature of the film and determines the in-plane epitaxial relationship between the film and the substrate: (100)[010]$SrRuO_3$//(100)[010]$SrTiO_3$. As shown in the 360° φ-scans (Fig. 1e), this in-plane epitaxial relationship is reflected in the mapping of the four-fold symmetry of the $SrTiO_3$(112) family of reflections (upper curve; K positive) onto the $SrRuO_3$ (112) family of reflections (lower curve). Since the Bragg reflections were sharp, well defined peaks, we performed a refinement of the lattice constants of the $SrRuO_3$ film. Using the following x-ray reflections: $SrRuO_3$ (002), (112), ($\bar{1}$ 12), (1$\bar{1}$ 2), ($\bar{1}\bar{1}$ 2), (022), (202), (0$\bar{2}$ 2), ($\bar{2}$ 02), (013), (103), (0$\bar{1}$ 3), and ($\bar{1}$ 03), we obtained lattice constants for the film of $a = b = c = 3.9400 \pm 0.001$Å, $\alpha = \beta = \gamma = 90.000 \pm 0.001°$ at room temperature. While the established crystal structure for $SrRuO_3$ is orthorhombic[14], the distortion of the cubic perovskite lattice is very small and our data corresponds well to the pseudo-cubic perovskite structure. The in-plane crystalline mosaic in the film is ~0.45°, which is determined from the FWHM of the φ-scans of the $SrRuO_3$ (112) reflection (Figs. 1d); the φ-scan of the $SrTiO_3$ (112) is shown for reference.

Using these $SrRuO_3$ thin films as bottom electrodes, epitaxial $Pb(Zr_xTi_{1-x})O_3$ (PZT; x=0, 0.35, 0.65) thin films were deposited layers on $SrTiO_3$ (100) and MgO (100) substrates by MOCVD. Using the growth conditions specified in Table I, the films produced were pure perovskite phase with a single-crystalline structure. Shown in Fig. 2 is the XRD data for two compositions of PZT films grown on epitaxial $SrRuO_3$(100) buffered $SrTiO_3$(100): PZT(0/100) [Fig. 2a, θ–2θ; Fig. 2b, θ-rocking for the (001) reflection; Fig. 2c, θ-rocking rocking for the (100) reflection] and PZT(35/65) [Fig. 2d, θ–2θ; Fig. 2e, θ-rocking rocking for the (002) reflection; Fig. 2f, θ-rocking rocking for the (200) reflection]. From the θ-2θ scans, Fig. 2a and 2d, we determine that the films have nominal compositions of $PbTiO_3$ and $Pb(Zr_{0.35}Ti_{0.65})O_3$, respectively, and are highly *c*-axis oriented. We have previously demonstrated that the presence of the PZT(0/100) and PZT(35/65) (100) reflections in the θ-2θ scans results from the presence of 90° domains (*a*-axis) in the films[6]. In addition, the films are epitaxial grown with respect to both the $SrRuO_3$ layer and the substrate. The θ-rocking of the PZT(0/100) (001) reflection (Fig. 2b), shows the presence of shoulders and consists of multiple peaks. This splitting arises as a result of the geometric and strain accommodation of the film when 90° domains are formed[15-16]. The θ-rocking of the PZT(35/65) (002) reflection (Fig. 2e), shows no splitting due to the better lattice mismatch and lower tetragonality of this composition combined with insufficient instrument resolution. The full width at half maximum for the PZT(0/100) (100), Fig. 2c, and PZT(35/65) (200), Fig. 2f, are 0.75° and 0.93°, respectively. From the integrated intensity ratio of the PZT(35/65) (002) and (200) reflections and the PZT(0/100) (001) and (100) reflections, we determine that the films contain a volume fraction of 90° domains of ~7% and ~29%, respectively.

Shown in Fig. 3 is the XRD data for two compositions of PZT films grown on epitaxial $SrRuO_3$(100)/$BaTiO_3$(001) buffered MgO(100): PZT(35/65) [Fig. 3a, θ–2θ; Fig. 3b, θ-rocking for the (002) reflection; Fig. 3c, θ-rocking rocking for the (200) reflection] and PZT(65/63) [Fig. 3d, θ–2θ; Fig. 3e, θ-rocking rocking for the (001) reflection]. From Fig. 3a-3c, we see that PZT(35/65) films grown on the buffered MgO substrates are quite similar structurally to those deposited on buffered $SrTiO_3$ (Figs. 2d-2f); however, with a slightly higher volume fraction of 90° domains of ~31%. From the θ-2θ scan of the PZT(65/35) film, we can see that the (001) and (100) reflections have merged indicating that the film has the

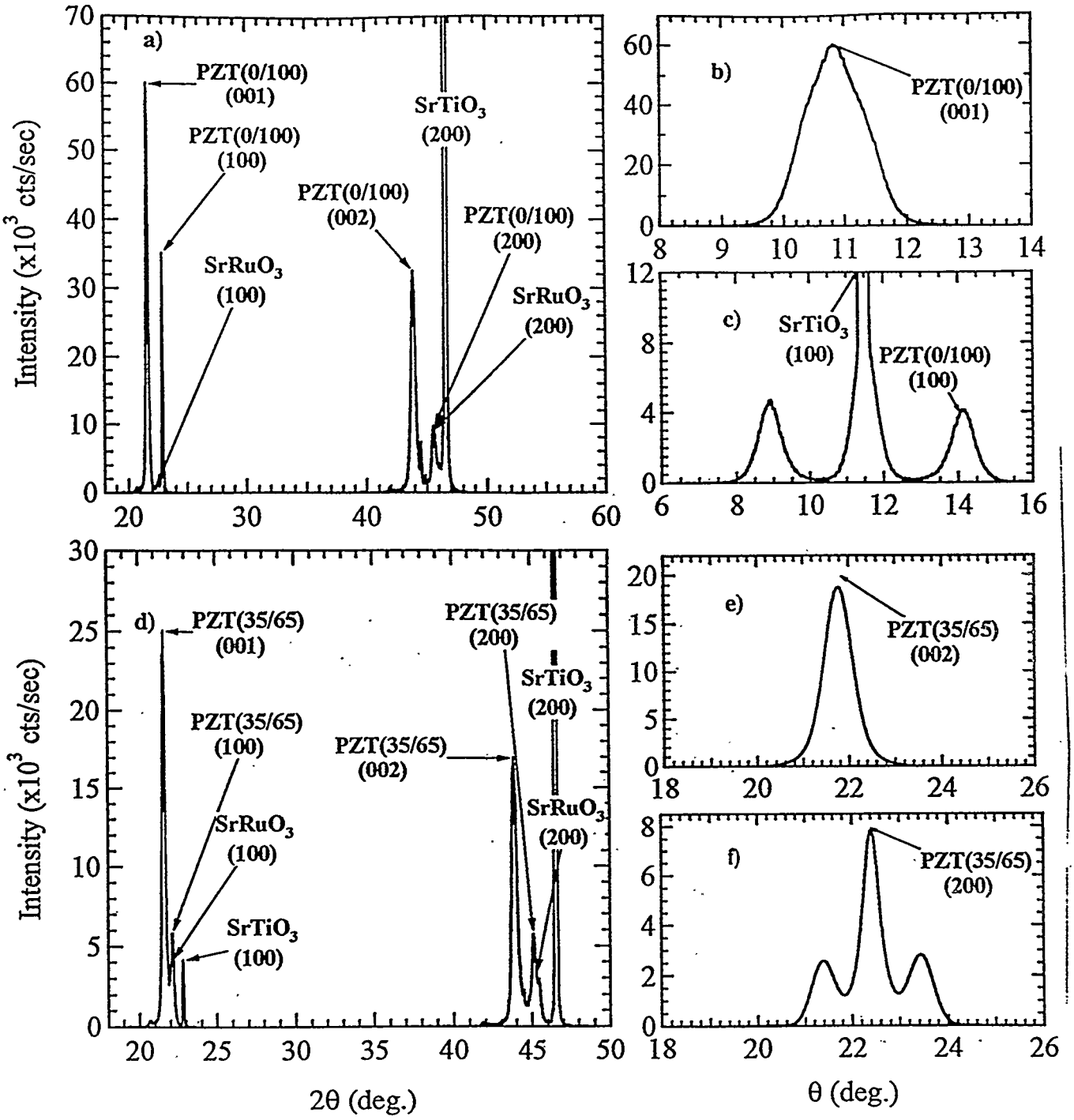

Figure 2. XRD data for two compositions of PZT films grown on epitaxial $SrRuO_3$(100) buffered $SrTiO_3$(100): PZT(0/100) [Fig. 2a, θ–2θ; Fig. 2b, θ-rocking for the (001) reflection; Fig. 1c, θ-rocking rocking for the (100) reflection] and PZT(35/65) [Fig. 2d, θ–2θ; Fig. 2e, θ-rocking rocking for the (002) reflection; Fig. 2f, θ-rocking rocking for the (200) reflection].

rhombohedral structure expected for this composition, and is (001) pseudo-cubic oriented (i. e., (012) rhombohedral); however, FWHM of the rocking curve of the PZT(65/35) (100) reflections is broad, ~1.6°, indicating that the degree of orientation of this film is poorer than that of tetragonal compositions.

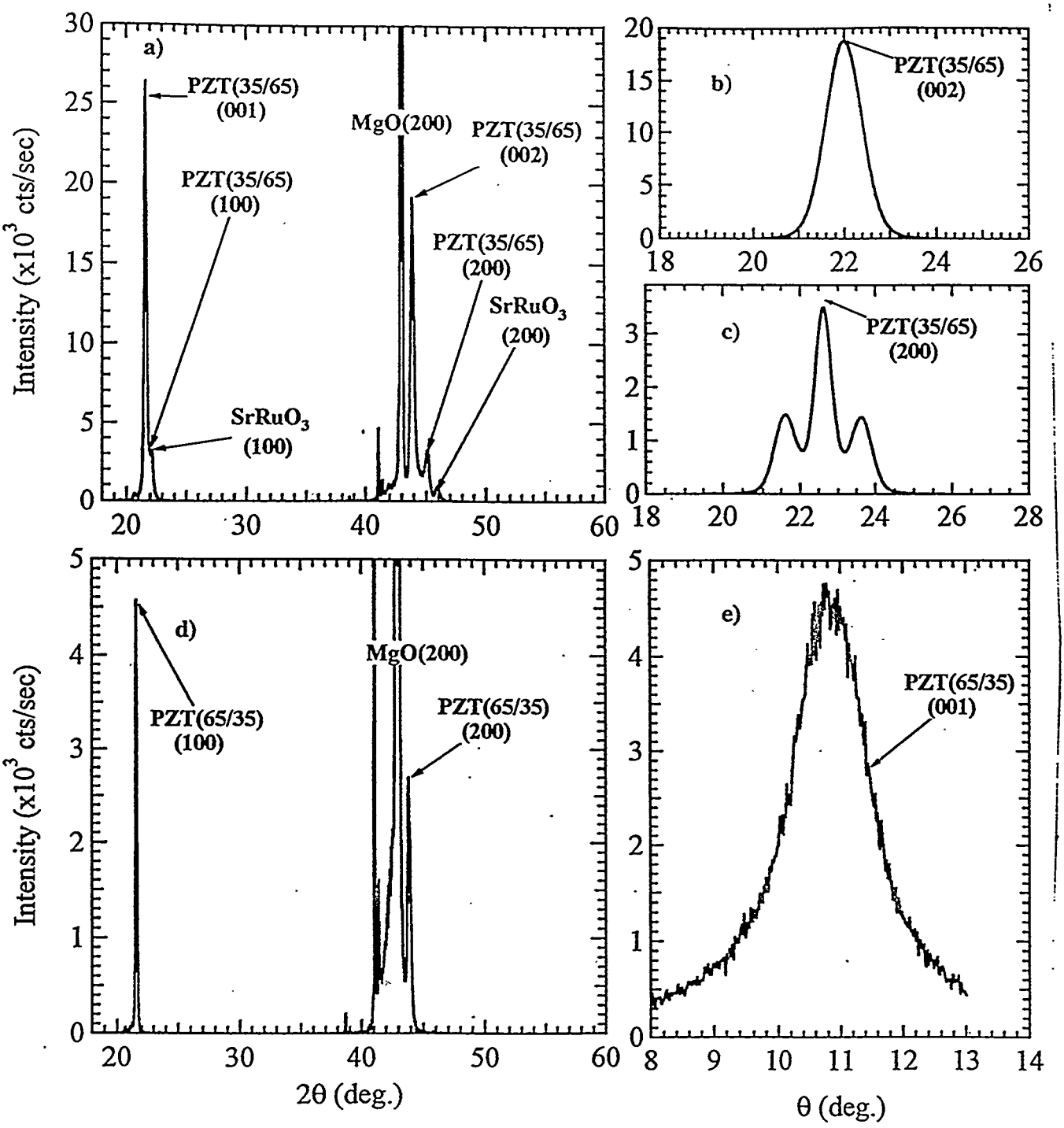

Figure 3. XRD data for two compositions of PZT films grown on epitaxial $SrRuO_3$(100)/$BaTiO_3$(001) buffered MgO(100): PZT(35/65) [Fig. 3a, θ–2θ; Fig. 3b, θ-rocking for the (002) reflection; Fig. 3c, θ-rocking rocking for the (200) reflection] and PZT(65/63) [Fig. 3d, θ–2θ; Fig. 3e, θ-rocking rocking for the (001) reflection].

In Fig. 4a, we show the results of RBS channeling measurements on the $Pb(Zr_{0.35}Ti_{0.65})O_3$ grown directly on $SrTiO_3$(100), the maximum channeling yield reduction at the Pb signal is ~71%. The inset of Fig. 4a shows the angular channeling width; the full width at half minimum is ~1.6°. In fig. 2b, we show the RBS

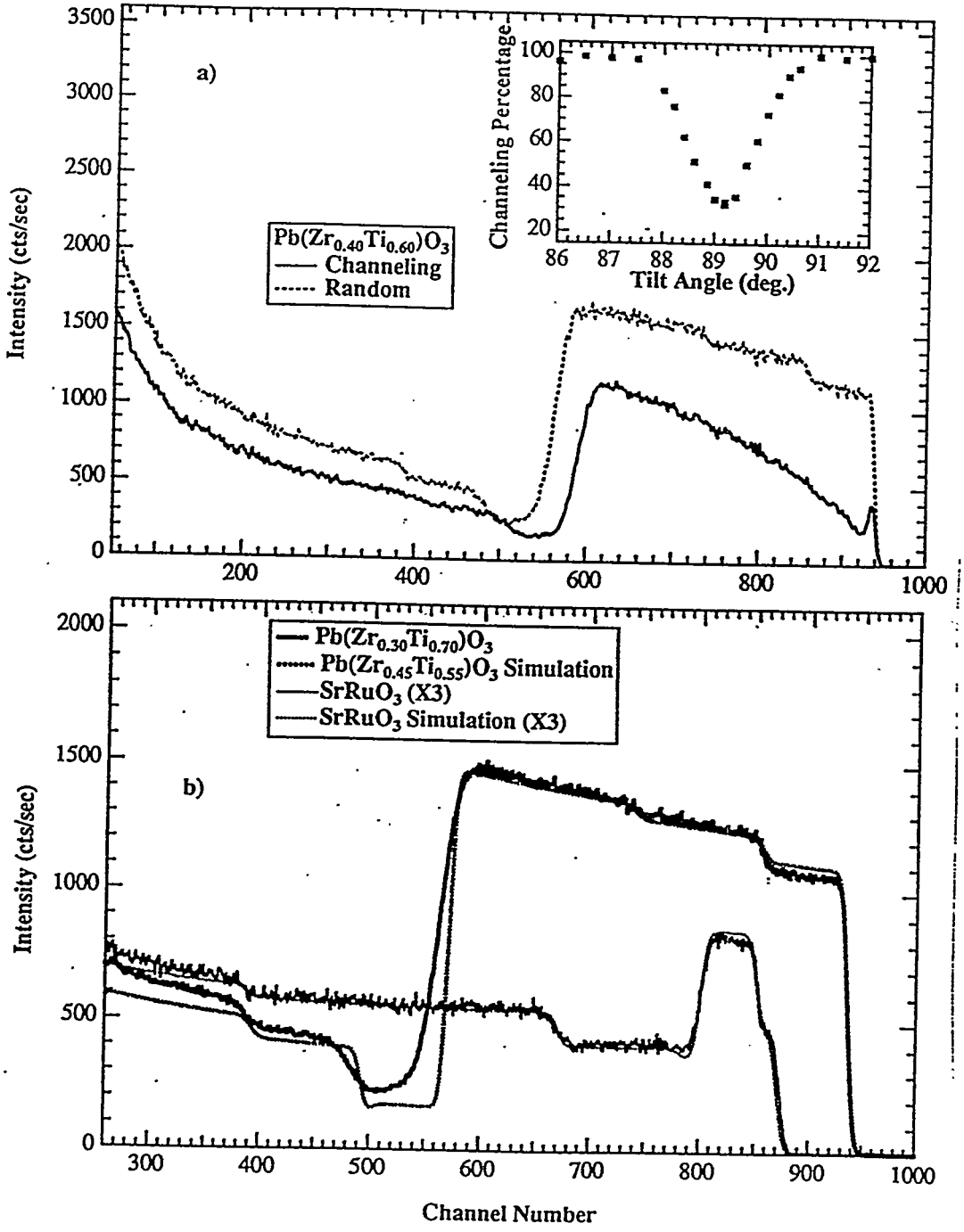

Figure 4. a) RBS channeling results for an epitaxial $Pb(Zr_{0.35}Ti_{0.65})O_3$ thin film grown on $SrTiO_3(100)$. The inset shows the angular channeling width. b) RBS data and simulation results for epitaxial $Pb(Zr_{0.35}Ti_{0.65})O_3$ and $SrRuO_3$ thin films grown on $SrTiO_3(100)$.

data and simulations of the RBS data for a $Pb(Zr_{0.35}Ti_{0.65})O_3$ film grown directly on $SrTiO_3(100)$ and a $SrRuO_3$ film grown on $SrTiO_3(100)$. The simulation for the $SrRuO_3$ film indicates that the films is pure stoichiometric $SrRuO_3$ with a thickness of ~330Å. The simulation of the PZT film was less successful. The

best fit was obtained for a composition of PZT(45/55) (shown); however, the XRD and dielectric data (shown below) are more consistent with a composition of PZT(35/65); this issue remains unresolved.

In Fig. 5, we show the cross-section TEM image of a $PbTiO_3(001)/SrRuO_3(100)/SrTiO_3(100)$ epitaxial film. The image shows that the films is epitaxial *c*-axis oriented, with 90° domains and threadingdislocations being the primary structural defects. The thickness of the $SrRuO_3$ layer is ~330Å. Note that the 90° domain visible in the image clearly nucleates at structural defects in the substrate. The strain contrast associated with the substrate defect site appears to propagate directly through the $SrRuO_3$ layer into the $PbTiO_3$ layer. In addition, in lower magnification images, we observed threading dislocations that appear normal to the substrate/film interface and propagate through the 90° domains. Presumably, this would indicate that these dislocations form prior to the ferroelectric phase transition while the films is in the cubic state. The $PbTiO_3(001)/SrRuO_3(100)/SrTiO_3(100)$ interfaces shown in Fig. 5 are atomically sharp; note that the $PbTiO_3(001)/SrRuO_3(100)$ interface appears to be cleaner that the $SrRuO_3(100)/SrTiO_3(100)$ interface indicating that the deposition of the buffer layer appears to improve the quality of the substrate surface resulting in an improved ferroelectric film. The selected area electron diffraction pattern of the interface structure is shown as a inset to Fig. 5. This pattern determined the epitaxial relationships between the $PbTiO_3$ and $SrRuO_3$ films and the $SrTiO_3$ substrate: $(100)[010]PbTiO_3//(100)[010]SrRuO_3//(100)[010]SrTiO_3$. Optical waveguiding experiments showed that the $Pb(Zr_{0.35}Ti_{0.65})O_3(001)$ film had high ordinary refractive index of 2.5811 at 632.8 nm.

Shown in Fig. 6 are the results of polarization hysteresis (i. e., P-E curve) and polarization fatigue measurements of our PZT films. Fig. 5a shows the P-E curve for a Ag / PZT(35/65) (001) / $SrRuO_3(100)$ $SrTiO_3$ (100) capacitor. The results of these measurement are: a remanent polarization of 46.2 $\mu C/cm^2$, the saturation polarization of 55.1 $\mu C/cm^2$, a coercive field of 54.9 kV/cm, and a bipolar resistivity of $>5.8x10^9$ Ω-cm at 275 kV/cm. The dielectric breakdown strength of this capacitor was >400kV/cm (this field strength was the limit of our instrument). The dielectric constant of this films at 1 Mhz was 410. The electrical measurements indicate that the properties of this film are a significant fraction of those of bulk material (e. g., ~70% of the single crystal remanent polarization). However, we measured a volume fraction of 90° domains of ~30%. If we assume that only a small portion of this twin volume undergoes 90° switching, then this volume fraction of the film will not contribute to the measured remanent polarization; consequently, the true remanent polarization could be as high as ~60 $\mu C/cm^2$, very close to that of the bulk material at this composition. Fig. 5b shows the P-E curve for a Ag/PZT (65/35) $(001)/SrRuO_3(100)/SrTiO_3(100)$ capacitor. The results of these measurement are: a remanent polarization of 16.8 $\mu C/cm^2$, the saturation polarization of 20.4 $\mu C/cm^2$, a coercive field of 42.5 kV/cm, and a bipolar resistivity of $>1.5x10^{10}$ Ω-cm at 150 kV/cm. The dielectric breakdown strength of this capacitor was >250kV/cm (this field strength was the limit of our instrument). The dielectric constant of this films at 1 Mhz was 305. As show above, this film is (001) oriented; however, for rhombohedral compositions of PZT, the polarization axis is along the (111) pseudo-cubic direction. If we include this geometric factor, our actual remanent polarization along the (111) direction is 29.1 $\mu C/cm^2$. In addition, even though the fraction of ferroelectric domains in the material, unlike for tetragonal compositions, could not be measured by simple XRD, the films must contain some volume fraction of such material. These twins will also reduce the measured polarization values. In Fig. 5c, we show the result of polarization fatigue measurements of two Ag/PZT (65/35) $(001)/SrRuO_3(100)/SrTiO_3(100)$ capacitors in series. This data was taken at a pulse rate of 10 kHz and 15V. That data indicate that the

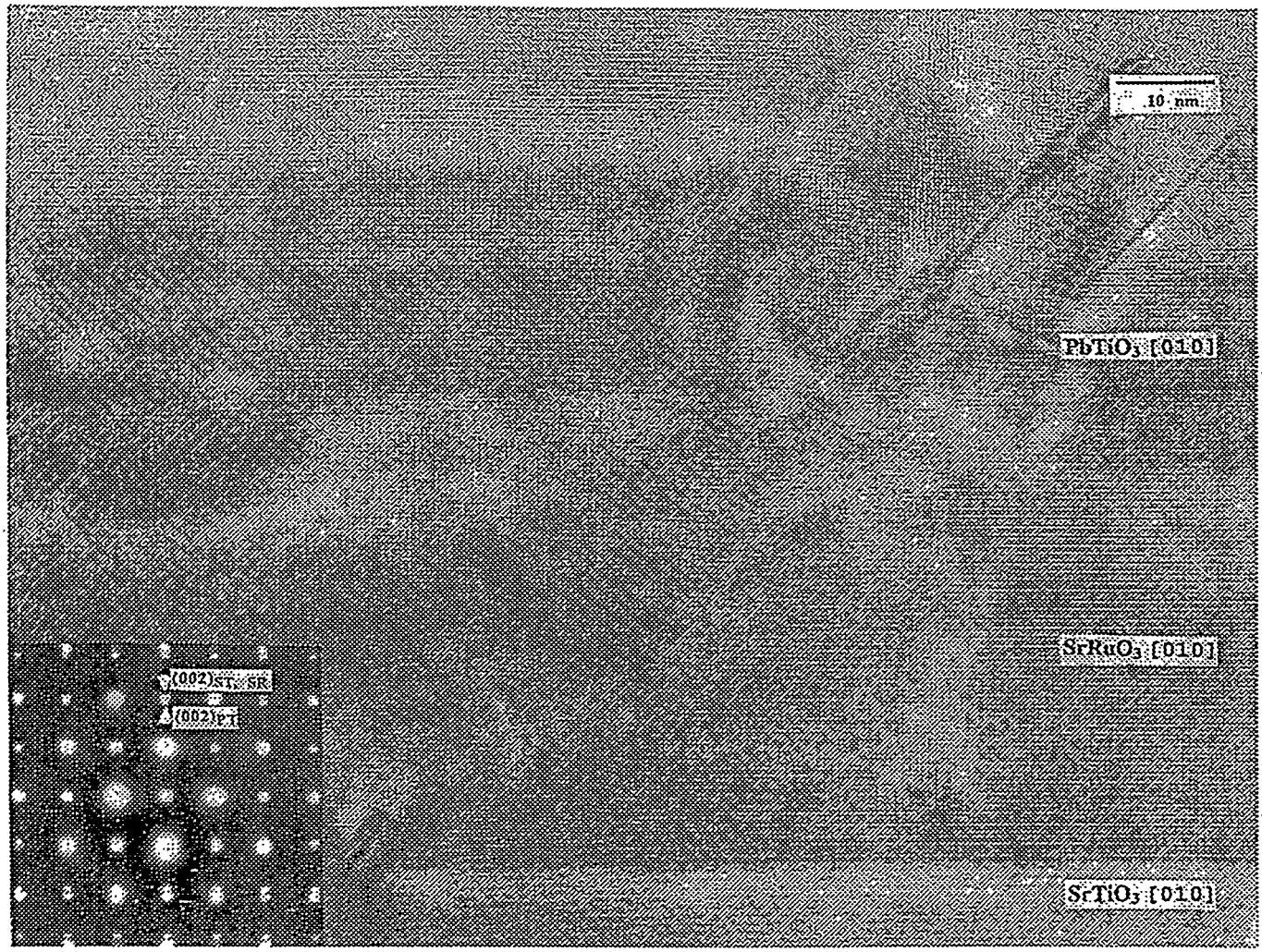

Figure 5. High resolution cross-sectional TEM image of the $PbTiO_3(001)$ / $SrRuO_3(100)$ / $SrTiO_3(100)$ interfaces showing that the individual layer interfaces are atomically sharp. The dominate defects in the film a 90° domains and threading dislocations. The inset shows the selected area electron diffration pattern of the interface region.

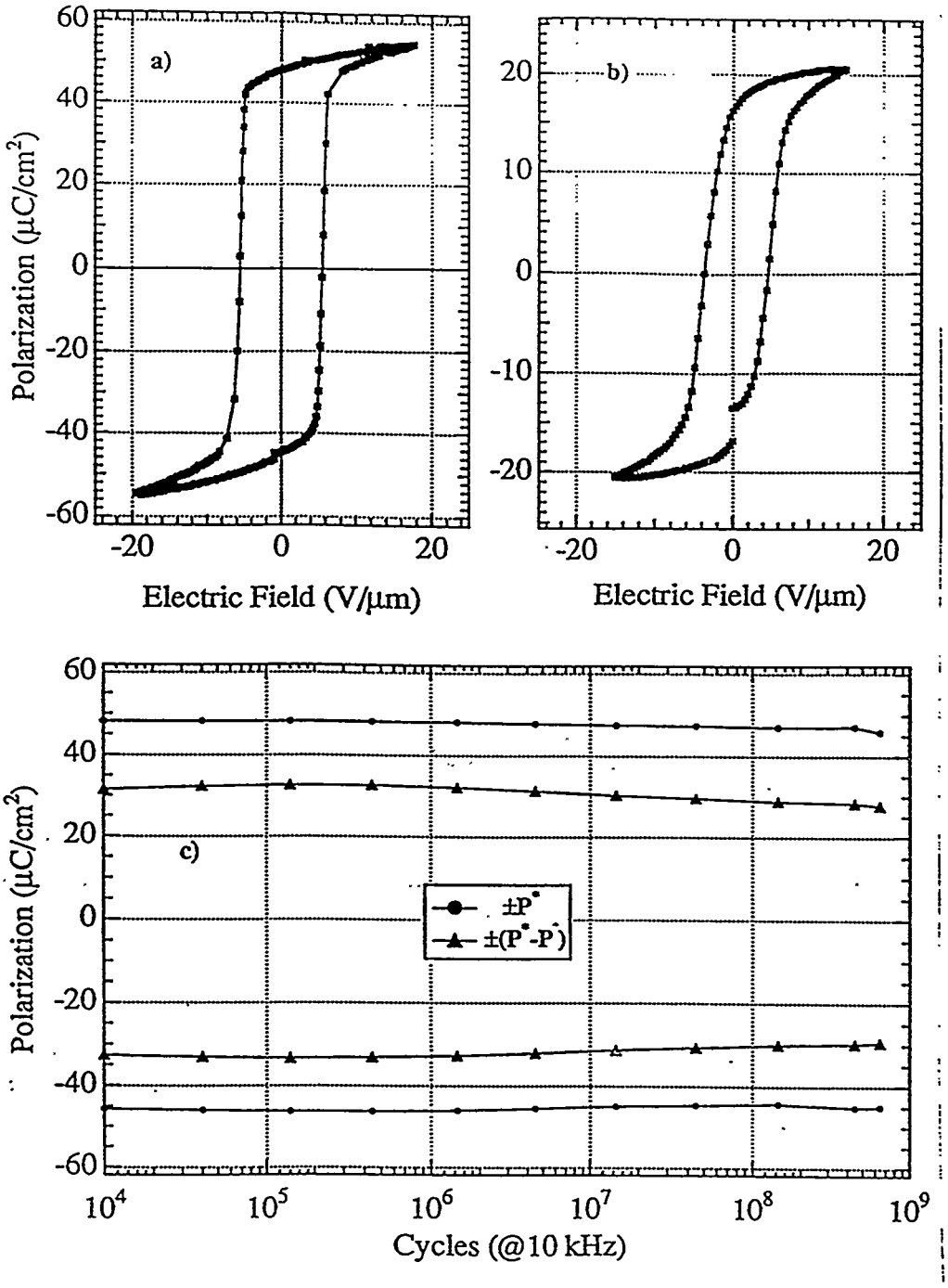

Figure 6. a) The ferroelectric polarization P-E hysteresis curve for a Ag / $Pb(Zr_{0.35}Ti_{0.65})O_3(001)$ /$SrRuO_3(100)$ / $SrTiO_3(100)$ capacitor. The ferroelectric polarization P-E hysteresis curve b) and polarization fatigue data c) for a Ag / $Pb(Zr_{0.65}Ti_{0.35})O_3(001)$ /$SrRuO_3(100)$ / $SrTiO_3(100)$ capacitor.

materials showed little fatigue out to 10^9 cycles. We note that the growth conditions for these PZT films have not been optimized and, in principle, improvements in the films crystallinity and properties could be achieved. These results indicate that through the use of epitaxial buffer layers and electrode materials, very high structural perfection can be achieved with commensurate bulk-like properties in epitaxial ferroelectric films.

3. ACKNOWLEDGMENTS

This work was supported by the U. S. Department of Energy, Basic Energy Science-Materials Science through contract #W-31-109-ENG-38 under the joint CRADA with Hewlett-Packard Company #C9301701.

4. REFERENCES

1. For example see, Ferroelectric Thin Films III, ed. E. R. Myers, B. A. Tuttle, S. B. Desu, and P. K. Larsen, (Mat. Res. Soc. Symp. Proc. Vol. **310**, San Francisco, CA 1993).
2. C. J. Brierley, C. Trundle, L. Considine, R. W. Whatmore, and F. W. Ainger, Ferroelectrics **90**, 181 (1989); A. I. Kingon, K. Y. Hsieh, L. L. King, S. H. Rou, K. J. Backmann, and R. F. Davis, in Ferroelectric Thin Films, ed. by E. R. Myers and A. I. Kingon, (Mat. Res. Soc. Symp. Proc. Vol. **200**, Pittsburg, PA 1990); T. Katayama, M. Fuzimoto, M. Shimizu, and T. Shiosaki, Jpn. J. Appl. Phys. **30**, 2189 (1991).
3. G. R. Bai, H. L. M. Chang, H. K. Kim, C. M. Foster, and D. J. Lam, Appl. Phys. Lett **64**, 408 (1992); Y. Gao, G. Bai, K. L. Merkle, Y. Shi, H. L. M. Chang, Z. Shen, and D. J. Lam, J. Mater. Res. **8**, 145 (1993).
4. G. R. Bai, H. L. M. Chang, C. M. Foster, Z. Shen, and D. J. Lam, J. Mater. Res. **9**, 156 (1994).
5. H. You, H. L. M. Chang, R. P. Chiarello, and D. J. Lam, in Heteroepitaxy of Dissimilar Materials, ed. by R. F. C. Ferrow, J. P. Harbison, P. S. Peercy, and A. Zangwill (Mat. Res. Soc. Symp. Proc. Vol. **221**, Pittsburg, PA 1990) p. 181.
6. C. M. Foster, Z. Li, G. R. Bai, H. You, D. Guo, and H. L. M. Chang, in Epitaxial Oxide Thin Films and Heterostructures, ed. D. K. Fork, J. M. Phillips, R. Ramesh, and R. M. Wolf, (Mat. Res. Soc. Symp. Proc. Vol. **341**, San Francisco, CA 1994).
7. C. M. Foster, Z. Li, M. Buckett, D. Miller, P. M. Baldo, L. E. Rehn, G. R. Bai, D. Guo, H. You and K. L. Merkle, (submitted to *J. Appl. Phys.*).
8. L. A. Wills and J. Amano, in Ferroelectric Thin Films IV (this work), presented at the 1994 Fall MRS Meeting, Boston, MA 1994).
9. C. M. Foster, S.-K. Chan, H. L. M. Chang, R. P. Chiarello, T. J. Zhang, J. Guo, and D. J. Lam, J. Appl. Phys. **73**, 7823 (1993).
10. H. You, H. L. M. Chang, R. P. Chiarello, and D. J. Lam, in Heteroepitaxy of Dissimilar Materials, ed. by R. F. C. Ferrow, J. P. Harbison, P. S. Peercy, and A. Zangwill (*Mat. Res. Soc. Symp. Proc.* Vol. **221**, Pittsburg, PA 1990) p. 181.
11. R. P. Sharma, L. E. Rehn, P. M. Baldo, and J. Z. Liu, Phys. Rev. Lett. **62**, 2869 (1989).
12. C. B. Eom, J. M. Phillips and R. J. Cava, in Epitaxial Oxide Thin Films and Heterostructures, ed. D. K. Fork, J. M. Phillips, R. Ramesh, and R. M. Wolf, (Mat. Res. Soc. Symp. Proc. Vol. **341**, San Francisco, CA 1994).
13. H. N. Al-Shareef, A. I. Kingon, X. Chen, K. R. Bellur, and O. Auciello, *J. Mater. Res.* **11**, 2968 (1994).
14. X-ray Powder Diffraction Data Card, JCPDS 43-472.
15. W. Pompe, X. Gong, Z. Suo, and J. S. Speck, *J. Appl. Phys.* **74** (10), 6012 (1993); J. S. Speck and W. Pompe, J. Appl. Phys. 76 (1), 466 (1994).